Imaging Ca2+ Concentration and pH in Nanopores/Channels of Protein Crystals

THE JOURNAL OF PHYSICAL CHEMISTRY B

Article

Cite This: J. Phys. Chem. B 2018, 122, 9646−9653

pubs.acs.org/JPCB

Imaging Ca^{2+} Concentration and pH in Nanopores/Channels of Protein Crystals

Kazuo Mori* and Bernd Kuhn*

Okinawa Institute of Science and Technology, Graduate University, 1919-1 Tancha, Onna-son, Okinawa 904-0495, Japan

ABSTRACT: Protein crystals are nanoporous materials. Despite this important characteristic, little is known about the conditions in the pores, also called channels. Here, we describe a method to study the calcium concentration and pH in the nanopores of thaumatin and lysozyme crystals. We load the crystal nanopores with fluorescent indicators and then perfuse the crystals with solutions of different calcium concentrations and pH while reading out the crystal's fluorescence intensity with confocal microscopy. By calibrating the fluorescence signal, we can determine the calcium concentration and pH in the nanopores. For the pH in thaumatin nanopores measured with the ratiometric pH sensor SNARF-1, we find a −0.7 pH shift compared to the bath pH corresponding to a fivefold higher proton concentration. This is similar to the −0.3 pH shift found in lysozyme nanopores. With single-wavelength probes, we find that the calcium concentration in thaumatin crystal nanopores is the same as in the bath, whereas it is 0.24 times lower in lysozyme nanopores. Summarizing, our experiments show that calcium concentration and pH in the nanopores of protein crystals can deviate significantly from that in the bath. In general, the described method can be applied for testing a wide range of ion or small-molecule concentrations in transparent nanoporous materials not only with ratiometric but also with single wavelength fluorescent indicators.

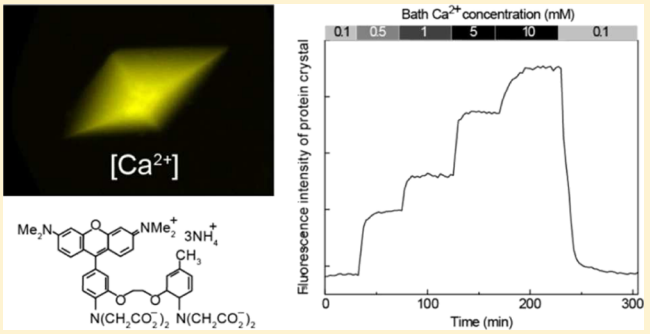

INTRODUCTION

A crucial method to reveal protein structure is X-ray crystallography of protein crystals formed in aqueous solutions. As large protein molecules cannot be stacked in a space-filling way, water-filled nanopores, also called channels, are formed between the molecules. These pores can come in a wide range of sizes and shapes, and the water content of a protein crystal can range from 30 to 70%.[1] Because of the hindered diffusion in nanopores, the concentration of small molecules or ions is not expected to be the same as in the bath. However, for protein structure analysis as well as for the applications of protein crystals as nanoporous materials, it is important to know the specific conditions, such as pH or ion concentration, in the pores.

It was shown before that protein crystals can be labeled with fluorescent dyes by binding the dye covalently to the protein,[2−4] by growing the crystal in a solution containing dye,[5] or by soaking the crystal in a dye solution.[6−10] If the dye is covalently bound to the protein, the dye will be fixed in the crystal. Also, in the case of growing the crystal in a solution containing dye, the dye will be at least partly integrated into the crystal structure. In the case of soaking the crystal in a dye solution, the fluorescent dye molecules enter the nanopores by diffusion.[11,12] This is possible because of their relative small size compared to the size of protein molecules and the resulting pore size. As small protein crystals are typically transparent in visible light, the dyes allow not only imaging the crystal surface but also its interior with fluorescence microscopy, including confocal[6,9,13] and two-photon excited fluorescence microscopy (in short, two-photon microscopy).[10,14]

In addition to labeling the protein crystals with dyes for visualization, also functional dyes can be used, for example, to measure the pH in the nanopores of a protein crystal.[10] In general, a wide range of molecular probes were developed for chemical sensing (see, for example, Chapter 14 in *Molecular Fluorescence*[15]). Sensors are available not only for pH, metal ions, and anions, but also for some neutral molecules and gases.

In a previous paper,[10] we showed that it is possible to measure the pH in lysozyme crystals. We were able to follow pH changes in the crystal nanopores three-dimensionally resolved with two-photon microscopy. Interestingly, we found a pH in the crystal which was 0.3 lower than that in the bath solution. One of the major experimental difficulties was to change the bath solution slow enough to avoid cracking and dissolving of the protein crystals.

In this article, we describe a simple perfusion chamber which allows slow changes of solutions. In addition to pH measurements, we show that also calcium concentrations can be measured in nanopores of protein crystals, as tested within thaumatin[16,17] and lysozyme[18,19] crystals. We describe our

Received: July 24, 2018
Revised: September 23, 2018
Published: October 11, 2018

DOI: 10.1021/acs.jpcb.8b07099
J. Phys. Chem. B 2018, 122, 9646−9653

experience with the experiments to help avoid common pit falls and problems.

METHODS

Lysozyme Crystals. Lysozyme was crystalized, as described before.[10] In short, lysozyme (Sigma) was dissolved 50 mg/mL in 50 mM acetate buffer. A 1:1 mixture of protein solution (10 μL) and the precipitant (1 M sodium chloride, 50 mM acetate buffer, pH 4.5) was filtered (0.22 μm) and then placed into the crystallization chamber of the crystal growth chamber (MVD/24, Charles Supper) for sitting-drop crystallization. The precipitant (500 μL) was used in the reservoir. The chamber was kept at 4 °C. Crystals stopped growing after 2 weeks. The tetragonal crystals were typically smaller than 300 μm. After the growth was completed, the crystals were stored at room temperature (24 °C).

Thaumatin Crystals. Thaumatin was crystalized following the recipe of Rigaku (https://www.rigaku.com/en/products/protein/recipes): thaumatin (Sigma or Alfa Aesar) was dissolved 50 mg/mL in distilled water. A 3:2 mixture of protein solution (10 μL) to precipitant [NaK tartrate (24% w/v), ethyl glycol (15% v/v), 0.1 M bis tris propane, pH 6.5] was filtered (0.22 μm) and placed on the lid of a crystal growth chamber (Cryschem Plate, Hampton Research) for hanging-drop crystallization. The precipitant (500 μL) was used in the reservoir. The tetragonal crystals grew at 4 °C for 2 weeks to a size of typically less than 300 μm. Then, the chamber with crystals was stored at room temperature.

Labeling of Crystals. For measurement of the conditions in the nanopores of protein crystals, the pH-sensitive dye SNARF-1 (Molecular Probes, pK_a 7.5) and the Ca^{2+} sensitive dyes Rhod-5N tripotassium salt (AAT Bioquest, K_d: 320 μM, MW 900.02), Fluo-5N pentapotassium salt (Molecular Probes, K_d: 90 μM, MW 958.0582), Rhod-FF tripotassium salt (AAT Bioquest, K_d: 19 μM, MW 891), and Rhod-2 triammonium salt (Biotim, K_d: 1 μM, MW 806) were used. Stock solutions were prepared at a concentration of 1 mM in water and diluted in a precipitant to a 0.01 mM staining solution.

Lysozyme crystals were labeled with SNARF-1 and Rhod-2 by immersing the crystals in staining solution (0.01 mM) containing lysozyme (1 mg/mL). The crystals were homogeneously labeled after 5 days.

Thaumatin crystals labeled and unlabeled much faster than lysozyme. Therefore, we added the fluorescent dyes only to the bath solutions (0.01 mM) with different pH or Ca^{2+} concentrations during imaging.

Perfusion Chamber and Perfusion Solutions. The imaging experiments were performed in a perfusion device (Figure 1). This device was made of a 3 mm thick silicone layer (Sylgard, Dow Corning, about 2 × 4 cm) on a glass slide with an embedded silicone tubing (0.5 mm inner and 0.6 mm outer diameter) passing through the long axis. After the silicone cured, an oval-shaped chamber was cut out which can hold about 20 μL solution so that the embedded tubing formed an inlet and outlet.

We used two syringe pumps (Pump 11 Elite 70-4500, Harvard Apparatus) to perfuse the chamber with different bath solutions. To measure pH in the crystal, we prepared bath solutions with pH 7.0, 7.5, 8.0, 8.5, and 9.0 calibrated with a pH meter (9615S-10D and F-72, HORIBA). Pumps were connected to the chamber through three 3-way stopcocks to prevent bubbles from entering the perfusion chamber (Figure 1).

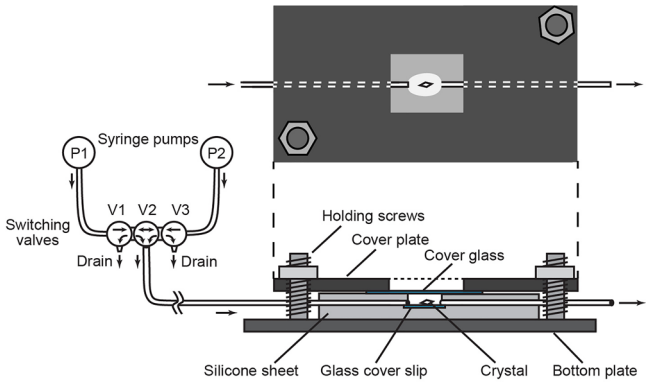

Figure 1. Schematic drawing of the protein crystal perfusion system used for imaging. Two syringe pumps P1 and P2 drove the test solutions through the perfusion chamber. To prevent air bubbles, three 3-way stopcocks V1, V2, and V3 were inserted at the tubing junction (see Methods). The perfusion device was composed of a silicone sheet (2 × 4 cm, 3 mm thick) with embedded cover glass, tubing, and oval perfusion chamber, and an aluminum base and cover plate clamped together by two screws to seal the chamber with a glass coverslip. For the perfusion experiment, one or more crystals were placed in the oval chamber with about 20 μL of precipitant before closing and sealing the chamber.

For calcium measurements, $CaCl_2$ (Sigma) was dissolved in the dye-containing (0.01 mM) bath solution at concentrations of 0.01, 0.05, 0.1, 0.5, 1.0, 5.0, and 10 mM for Rhod-2 and 0.1, 0.5, 1.0, 5.0, and 10 mM for all other Ca^{2+} sensitive dyes. Thaumatin bath solutions with Ca^{2+} concentration higher than 15 mM precipitated, but the lysozyme bath solution did not. Therefore, we also used a lysozyme bath solution with 20 mM $CaCl_2$.

Microscope. Crystals were imaged with a confocal microscope (LSM 710, Zeiss) with a 20× objective (N.A. 0.4, Zeiss). SNARF-1 was excited at 488 nm with typically 30 μW measured at the objective front lens, and two emission bands (549−610 nm and 616−724 nm) were detected to allow ratiometric pH measurement. Rhod-2, Rhod-5N, and Rhod-FF were excited at 543 nm with typically 10 μW measured at the objective front lens and fluorescence was detected between 558 and 606 nm, and Fluo-5N was excited at 488 nm with typically 30 μW measured at the objective front lens and fluorescence was detected between 510 and 540 nm. The pin hole was set to 1 airy unit for all recordings. The microscope was controlled by Zen software (Zeiss).

Imaging of Protein Crystals. Crystals were transferred from the growth chamber to the perfusion chamber with a micro sling (Crystal Cap Copper HT, 0.1−0.2 mm Cryo Loop; HR8-175, Hampton Research). Then, the perfusion chamber (Figure 1) was filled with bath solution. After transfer, the chamber was closed with a cover glass. Care was taken such that no air bubbles were in the chamber and that the crystals did not crack because of osmotic shock or drying. Also, care was taken such that the perfusion was not too strong to wash away the crystals. This was tested in preliminary experiments. The switching between the two pumps can easily introduce bubbles into the perfusion chamber. This can easily be avoided by using three 3-way stopcocks (Figure 1). For example, when switching from P2 to P1, the solution of P1 is directed through V1 to V2 and drained at V3 until all bubbles are removed. Then, the bubble-free solution is passed through V1 and then

DOI: 10.1021/acs.jpcb.8b07099
J. Phys. Chem. B 2018, 122, 9646−9653

from V2 to the chamber. When switching back to P2, the solution which might contain bubbles is drained at V1.

Lysozyme crystals were labeled for at least 5 days before the experiment and were therefore ready for imaging immediately after mounting.

Thaumatin crystals were not labeled beforehand to measure at first the autofluorescence in precipitant. Then, the perfusion solution was switched to the precipitant solution with 0.01 mM dye. The fluorescence intensity of the dye in the crystal was periodically imaged every 2.5 or 5 min until the intensity reached a plateau.

pH and Ca^{2+} measurements followed the labeling process by imaging one or more crystals simultaneously. Crystals were three-dimensionally reconstructed with confocal microscopy to find the crystal's midpoint. Fluorescence images with 512 × 512 pixels were taken through the center of the crystals with 166 ms/frame every 2.5 or 5 min. After switching to a new solution, we imaged until the fluorescence intensity reached a plateau, indicating equilibrium. Then, we switched to the next solution until imaging was completed in all prepared solutions. Stacks were taken with 1 μm z-spacing.

Analysis of Imaging Data. The mean fluorescence intensities were obtained from different regions of interest (ROIs) of the crystals and the bath solution using FIJI.[20] Background intensities were measured from an ROI in the bath before adding dye to the bath and subtracted from the intensities of the bath after dye application and SNARF-1-labeled crystals. For thaumatin crystals, either the background measurement was subtracted to show the autofluorescence or the autofluorescence measurement was used as the background measurement and subtracted from the crystal intensities after labeling to extract the fluorescence of the functional dye. To reduce noise, intensities used for further analysis were averaged over a time window when equilibrium was reached (typically 4 frames). Intensity ratios were calculated from the corrected intensities.

Determination of pH in Crystal Nanopores. After background and autofluorescence correction, intensity ratios of the two SNARF-1 fluorescence bands were calculated (Origin, Origin Lab). The bath intensity ratios were used as a calibration curve to determine the pH in the crystal. The bath intensity ratios were linearly interpolated.

Determination of Calcium Concentrations in Crystal Nanopores. Because of the high salt concentration in the bath, the K_d of the calcium-sensitive dye is different from the K_d determined in physiological solutions and has to be determined before estimating the calcium concentration in the nanopores. The K_d of the dye in the bath solution was obtained by fitting the function

$$I_{bath}([Ca^{2+}]) = \frac{[Ca^{2+}]}{(K_d + [Ca^{2+}])}$$

to the data, where I_{bath} is the intensity of the dye-containing bath and $[Ca^{2+}]$ is the calcium concentration of the solution.[20] The possible Ca^{2+} scaling factor α in the crystal was obtained by fitting the crystal intensity $I_{crystal}$ using the above-determined K_d and the calcium concentration $[Ca^{2+}]$ of the bath with the function

$$I_{crystal}([Ca^{2+}]) = \frac{\alpha[Ca^{2+}]}{(K_d + \alpha[Ca^{2+}])}$$

This was done under the assumption that the K_d of the calcium indicator in the bath solution is the same as in the protein crystal nanopores.

RESULTS

Labeling and Delabeling of Thaumatin Crystals. Thaumatin crystals (Figure 2A) were labeled by perfusing them with the precipitant containing 0.01 mM dye in the perfusion chamber (Figure 2B). The crystals did not show any color change because of the labeling when observed by eye in a wide-field microscope. Only after labeling with a 10-times higher dye concentration, the labeling becomes visible (Figure 2C). However, the crystals labeled with 0.01 mM bath solution showed bright fluorescence (Figure 2D). We imaged the time course of the dye diffusing into the crystals starting from autofluorescence as the baseline (Figure 2E,F). The fluorescence intensity gradually increased and finally reached a plateau. The labeling time constants τ_1 and τ_2 were obtained by fitting with a single or double exponential function

$$y = y_0 + A_1\, e^{-x/\tau_1} + A_2\, e^{-x/\tau_2}$$

We find SNARF-1 (16 min), Rhod-FF (18 min, 273 min), Rhod-2 (13 min, 340 min), Rhod-5N (19 min, 6.2 min), and Fluo-5N (8.6 min).

By perfusing the labeled thaumatin crystals with dye-free precipitant, it was also possible to image the time course of delabeling (Figure 2F). The fluorescence intensity returned to the original autofluorescence level. The delabeling time constants τ_1 and τ_2 were obtained by fitting a single or double exponential function

$$y = y_0 + A_1\, e^{-(x-x_0)/\tau_1} + A_2\, e^{-(x-x_0)/\tau_2}$$

We found SNARF-1 (16 min), Rhod-FF (0.3 min, 12 min), Rhod-2 (20 min, 150 min), and Fluo-5N (12 min). As the dyes were washed out at similar rates as they were washed in, thaumatin crystals did not bind or incorporate dye molecules.

To show the time course of dye diffusion into the crystal, we plot profiles across the crystal surface (Figure 2G). Starting from autofluorescence, the fluorescence intensity increased at first at the crystal surface after the bath solution was switched from the dye-free precipitant to the precipitant-containing dye. With time, also the center of the crystal got labeled and finally reached a plateau. Fluorescence intensities of the labeled crystals were always higher than the intensity of the bath solution. This indicates that dye molecules are accumulated in the crystal, as shown before in lysozyme crystals.[10] To compare the dye concentration in the crystal nanopores and the bath solution (0.01 mM dye concentration), we calculated the ratio of fluorescence intensities (Figure 2H). The intensities of Rhod-2, Rhod-FF, Rhod-5N, and Fluo-5N were 16-fold, 9.5-fold, 6.9-fold, and 5.2-fold higher in the crystal than in the bath, respectively.

pH in Thaumatin Crystal. The pH in crystals was measured by using the pH-sensitive dye SNARF-1 (Figure 3). The pH of the crystal bath solution was changed by perfusing it with SNARF-1-containing precipitant adjusted to a pH of 7.0, 7.5, 8.0, 8.5, and 9.0. Fluorescence was collected in a red (616−724 nm) and an orange (549−610 nm) emission band (Figure 3A). Ratiometric images were obtained by dividing the red by the orange intensities in different pH bath solutions (Figure 3B−D). The fluorescence intensity was recorded every 5 min for 5 h (Figure 3E) to ratiometrically determine the pH

DOI: 10.1021/acs.jpcb.8b07099
J. Phys. Chem. B 2018, 122, 9646−9653

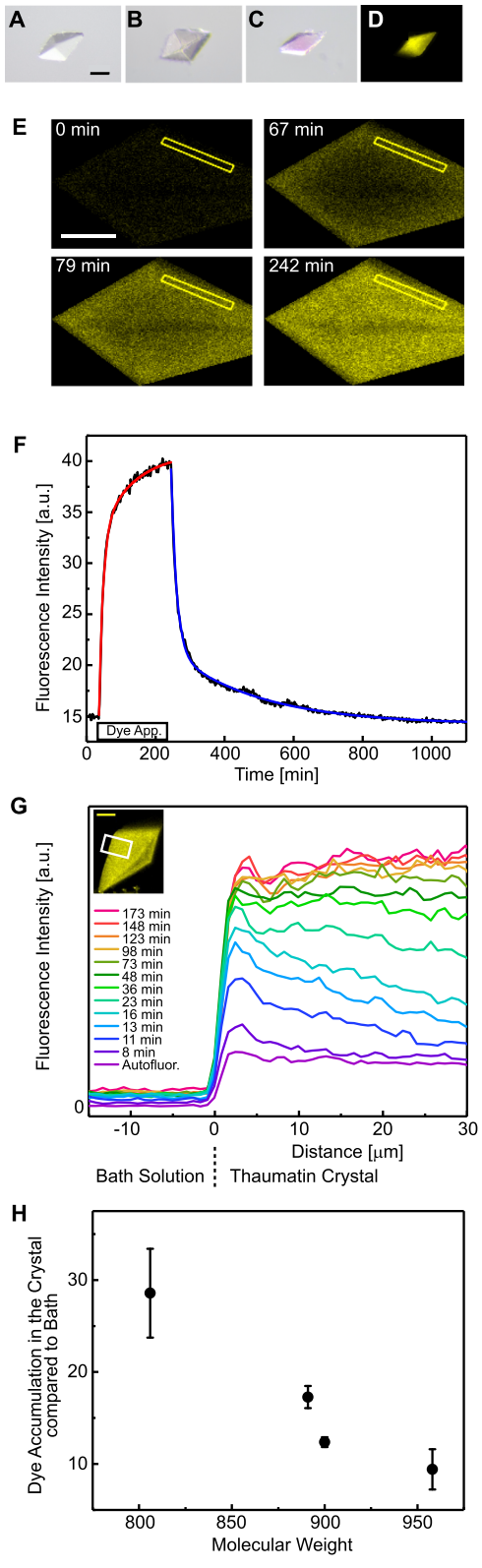

Figure 2. Labeling of thaumatin crystals with fluorescent dyes. (A) Bright-field image of a thaumatin crystal without labeling, (B) labeled with 0.01 mM of Rhod-2 as used for functional imaging, (C) labeled with 0.1 mM of Rhod-2, and (D) labeled with 0.01 mM Rhod-2 and imaged with a confocal microscope. (E) Fluorescence image of a thaumatin crystal during labeling with 0.01 mM Rhod-2. (F) Fluorescence intensity of a thaumatin crystal recorded at the ROI indicated in (E) during labeling and delabeling with the Ca^{2+} sensitive dye Rhod-2. Overlaid red and blue lines indicate the fittings for the labeling and delabeling. After delabeling, the fluorescence intensity recovered to the original intensity, suggesting that the dye was not or only weakly bound to the protein crystal. (G) Intensity profiles (average of the ROI indicated in the inset) at different time points after switching the perfusion from dye-free precipitant to precipitant-containing dye. The thaumatin crystal shows autofluorescence as many other protein crystals (magenta). After labeling the surface of the crystal, the dye diffuses into the core of the crystal until an equilibrium is reached. (H) Ratio of fluorescence intensity in thaumatin crystals and the bath solution (0.01 mM) shows that the thaumatin crystal accumulated the different dyes. Error bars represent standard deviation (Rhod-2: 9 crystals; Rhod-FF: 6 crystals; Rhod-5N: 7 crystals; Fluo-5N: 16 crystals). Scale bars in (A–D) indicate 100 μm and those in (E–H) indicate 50 μm.

in the crystal nanopores and in the bath (Figure 3F). We calibrate the pH in the crystal nanopores by comparing it with the intensity ratios of the bath (Figure 3G). Over a wide range of bath pH, the crystal nanopore pH was 0.7 lower than the pH of the bath, corresponding to a proton concentration in crystal nanopores that is fivefold higher than that in the bath solution. This is similar to the pH shift found in lysozyme nanopores.[10]

Ca^{2+} Concentration in Thaumatin Crystal Nanopores. To measure the Ca^{2+} concentration in the nanopores of thaumatin crystals, we perfused the crystals with precipitant containing 0, 0.05, 0.1, 0.5, 1.0, 5.0, or 10 mM Ca^{2+} and 0.01 mM calcium sensor dye.

We tested Rhod-5N (K_d: 320 μM), Fluo-5N (K_d: 90 μM), Rhod-FF (K_d: 19 μM), and Rhod-2 (K_d: 1 μM) to measure the Ca^{2+} concentration. The cited dissociation constants were determined under physiological conditions. However, in solutions with high ionic strength, the K_ds are expected to be different.

When we changed the Ca^{2+} concentration in the dye-bath solution, the equilibrium of the fluorescence intensity was reached within 30 min, whereas it required more than 2 h to keep the crystals in the dye-bath solution to label the thaumatin crystal with 0.01 mM of Rhod-2. By increasing the Ca^{2+} concentration from 0.1 to 10 mM, the fluorescence intensity increased (Figure 4A). When decreasing the Ca^{2+} concentration, the fluorescence intensity returned to the initially measured value indicating that Ca^{2+} is freely moving through the nanopores. Equilibrium was reached after 70 min. The equilibrium fluorescence intensity of the dye in the crystal was higher than that in the dye-containing precipitant (Figure 4B).

To estimate the calcium concentration in the nanopores of the crystal, we at first determined the K_d of the calcium-sensitive dye in the high osmotic strength bath solution. This was achieved by fitting a hyperbola to the measured equilibrium intensity of the bath over the applied bath calcium concentration (Figure 4C). The response curve of Rhod-2 was shifted to higher Ca^{2+} concentration (1.0 ± 0.2 mM, compared to 1 μM). We used the K_d of the bath solution and fitted the intensity measurements in the crystal nanopores with a hyperbola with a scaling factor for the calcium concentration which we call calcium scaling factor α. This was done under the assumption that the calcium concentration in the crystal scales with a constant factor compared to the calcium concentration in the bath. This assumption is plausible because of the constant shift of pH over a wide range which corresponds to a constant scaling factor. In the thaumatin

DOI: 10.1021/acs.jpcb.8b07099
J. Phys. Chem. B 2018, 122, 9646–9653

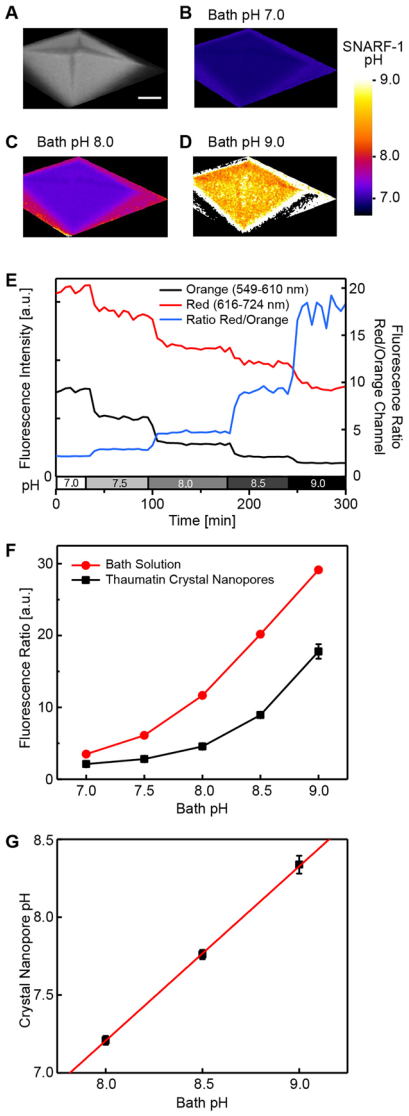

Figure 3. pH measurement in thaumatin crystals. (A) Fluorescence image (616−724 nm emission) of a thaumatin crystal labeled with SNARF-1. The scale bar indicates 50 μm. To visualize the pH in the crystal, the ratio of the 616−724 nm and the 549−610 nm emission bands was calculated. Ratiometric images of the crystal in bath solutions at (B) pH 7.0, (C) pH 8.0, and (D) pH 9.0 are shown. The color code was calibrated to pH by comparing to SNARF-1 fluorescence in bath solution. (E) Fluorescence intensities of the ratiometric pH-sensitive dye SNARF-1 in a thaumatin crystal in response to bath pH changes. (F) Fluorescence ratio of the crystal and the bath solution. The pH in the crystal nanopores is determined by comparing the crystal's fluorescence ratio with that of the bath solution. (G) pH difference between thaumatin nanopores and the bath is constant (ΔpH = −0.7). The lower pH in the nanopores indicates H^+ accumulation. Data points in (F,G) represent the mean of 6 crystals ± std.

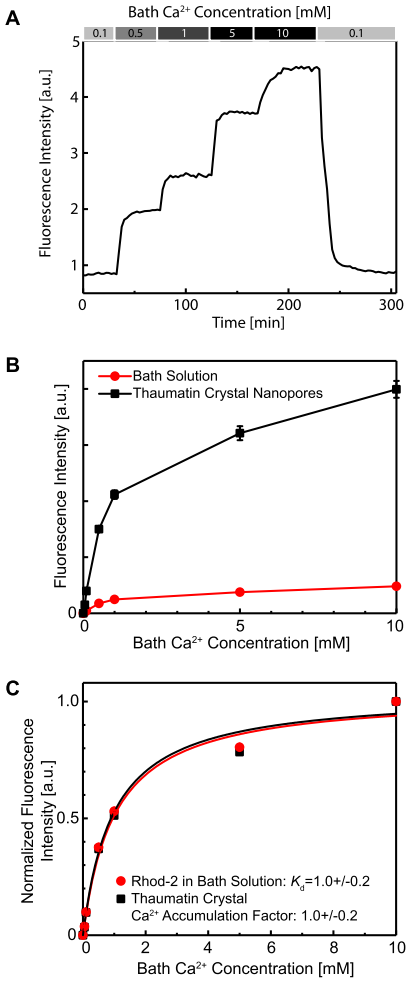

Figure 4. Ca^{2+} concentration measurement in thaumatin crystals. (A) Fluorescence intensity of Rhod-2 in a thaumatin crystal was changing with Ca^{2+} concentration change in the bath. Equilibrium of calcium change was reached about 30 min after the Ca^{2+} concentration change of the bath. (B) Equilibrium fluorescence intensities of Rhod-2 in a thaumatin crystal and the bath solution as a function of calcium concentration in the bath (average of 5 crystals ± std). (C) Normalized fluorescence intensities of Rhod-2 in the bath solution (red) are fitted by a hyperbola to obtain the K_d at the high ionic strength of the bath (1.0 ± 0.2 mM, average ± std). By using the K_d determined in the bath, the thaumatin crystal's calcium scaling factor is fitted (1.0 ± 0.2, average of 5 crystals ± std). Within the precision of the measurement, there is no difference in calcium concentration between the thaumatin nanopores and the bath.

crystal, this factor was 1.0 ± 0.2 (Figure 4C), and therefore we conclude that the calcium concentration in the bath and the nanopores of the crystal is the same within the accuracy of our measurement.

Labeling of Lysozyme Crystals. Lysozyme crystals are more fragile than thaumatin crystals. They crack and dissolve when exposed to physical or osmotic stress. To label lysozyme crystals, we added dye to a new well with precipitant and added 1, 5, and 10 mg/mL of lysozyme to reduce dissolving of the crystals. However, even with this method, about 25% of the crystals were immediately broken or dissolved just after they were moved into the solution, but about 50% of the surviving crystals lasted for more than a week. An increase of NaCl concentration from originally 1 M to up to 1.5 M did not improve this problem. To label lysozyme crystals, we kept the crystals in the solution with 0.01 mM Rhod-2 for typically 5 days. This long labeling time is similar to the labeling time of more than 72 h for the pH-sensitive dye SNARF-1.[10]

Ca^{2+} Concentration in Lysozyme Crystal Nanopores. Rhod-2-labeled crystals were placed into the experimental chamber, and the crystals were perfused with the precipitant containing 0, 0.5, 1, 5, 10, or 20 mM Ca^{2+} and 1 mg/mL lysozyme. Fluorescence intensities of the dye in lysozyme crystals were obtained in the same way as for the thaumatin

DOI: 10.1021/acs.jpcb.8b07099
J. Phys. Chem. B 2018, 122, 9646−9653

crystals, whereas those for the bath solution were obtained in separate experiments. We measured the intensities of six crystals with a confocal microscope (Figure 5A). As for the calcium measurement in thaumatin nanopores, we fitted at first the K_d of Rhod-2 in lysozyme-containing precipitant (0.89 ± 0.06 mM). Then, we determined the calcium scaling factor α in the lysozyme nanopores. In lysozyme crystals, α was 0.24 ± 0.02 (Figure 5B). We conclude that the calcium concentration in the lysozyme crystal nanopores is about a quarter of the calcium concentration in the bath.

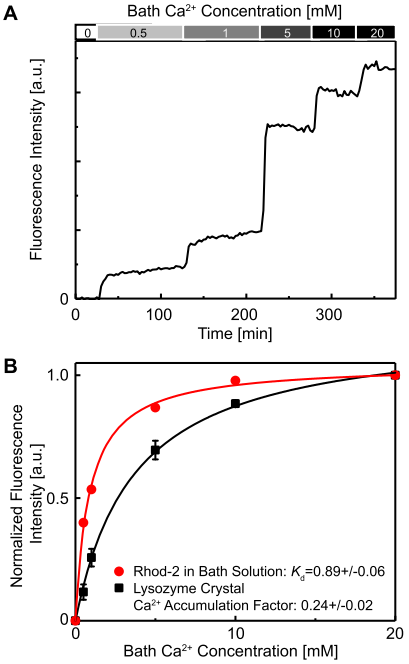

Figure 5. Ca^{2+} concentration measurement in lysozyme crystals. (A) Fluorescence intensity of a lysozyme crystal labeled with the calcium indicator Rhod-2 at different calcium concentrations of the bath. (B) Normalized fluorescence intensities of Rhod-2 in the bath solution (red) were fitted by a hyperbola to obtain the K_d in the high ionic strength bath solution (0.89 ± 0.06 mM, mean ± std). This K_d was used to infer the Ca^{2+} concentration in the lysozyme nanopores. The lysozyme calcium concentration factor is 0.24 ± 0.02 (average of 6 crystals ± std) indicating a reduced calcium concentration in the lysozyme nanopores compared to the bath.

DISCUSSION

In this article, we show that we can measure pH and Ca^{2+} concentration in the nanopores of thaumatin and lysozyme crystals with ratiometric and single-wavelength probes. We describe a method which allows to reliably and slowly exchange bath solutions to avoid cracking because of osmotic shock. We also show that by adding protein to the dye solution, it is possible to avoid dissolving of protein crystals during the perfusion.

Labeling of Crystals. Our labeling experiments show that thaumatin nanopores can be labeled and delabeled with different dyes within 300 min. This is significantly shorter than labeling lysozyme crystal nanopores that required more than 72 h for calcium-sensitive dyes Rhod-2 and the pH-sensitive dye SNARF-1.[10] Thaumatin crystals have pore sizes of 2.5−3.5 nm.[21] This pore size is significantly larger than the 1 nm pores of lysozyme crystals[19,22] and explains the faster diffusion of dye into the thaumatin crystal.

Because of the quick delabeling of thaumatin crystals, it was not possible to do the imaging experiments using dye-free precipitant for perfusion. To overcome this problem which might also occur in other crystals, we perfused the thaumatin crystals with precipitant containing a constant dye concentration. This kept the dye concentration in the thaumatin crystal constant.

The thaumatin crystal accumulates dyes as can be seen in an average intensity increase (Figure 2G). As the solvent content of the crystal is 56%,[21] the dye concentration in the nanopores is 1.8 times higher than that indicated by the intensity ratio. Therefore, the concentration of Rhod-2, Rhod-FF, Rhod-5N, and Fluo-5N is 29-fold, 17-fold, 12-fold, and 9-fold higher in the crystal than in the bath (0.01 mM), respectively. The resulting dye concentrations are low enough to exclude dye−dye interaction. The crystal nanopores are also far away from saturation with dye molecules.

Thaumatin nanopores accumulate less dye in comparison with lysozyme crystals (760-fold higher than in the bath).[10] This can be explained by a slower diffusion of the dye in lysozyme crystals because of the smaller pore size.[10]

Lysozyme was more difficult to label because it is much more fragile. Even with increased ion concentration, the crystals melted when adding dye solution. Therefore, it was helpful to also dissolve protein in the labeling and perfusion solution to reduce the dissolution of the crystal. A slow and gradual change in pH also increased the success rate significantly by avoiding cracks.

In general, some protein crystals show strong absorption and/or autofluorescence, such as ferritin and thaumatin. This makes the fluorescence experiments more difficult and requires subtraction of the autofluorescence to avoid misleading results.

Interestingly, all dye−crystal combinations we tried resulted in labeling of the crystals. We expect that this can be generalized for most synthetic dye−protein crystal combinations and therefore open the method for a wide field of applications.

pH Measurement in Crystal Nanopores. Protein crystals have a high water content of typically 30−70%.[1] This high water content allows defining a pH in the nanopores of the crystal. This pH can be measured by diffusing molecular probes into the crystal nanopores and then by reading out the pH optically.[10]

The pH in the nanopores of thaumatin crystals was lower than that in the bath solution. We found a constant pH difference to the bath of $\Delta pH = -0.7$. This indicates a fivefold accumulation of protons in the crystal nanopores in the range of pH 8−9. The average pH shift in lysozyme crystals was $\Delta pH = -0.3$ corresponding to a doubled proton concentration compared to the bath (Figure 4 in ref 10).

Calcium Measurement in Crystal Nanopores. The estimate of the calcium concentration in the crystal nanopores is based on the assumption that the K_d in the bath and in the nanopores is the same. This assumption is plausible as the dyes can be easily washed in and out of the crystal, and therefore there is no strong interaction between the crystal and the dye molecule which could alter the behavior of the functional properties of the dye.

The change of calcium concentration in a crystal occurs quite rapidly (30 min to reach equilibrium) corresponding to a nonhindered diffusion of Ca^{2+} in the nanopores. Concluding

DOI: 10.1021/acs.jpcb.8b07099
J. Phys. Chem. B 2018, 122, 9646−9653

from a model that requires hindered diffusion for accumulation,[10] no difference between bath calcium concentration and calcium concentration in the nanopores is expected. The experimental results confirm this prediction, and we find no difference in calcium concentration in the precipitant and the pores of thaumatin.

For lysozyme which has smaller nanopores than thaumatin, we find that the calcium concentration in equilibrium is only 24% of that in the bath over a wide range of calcium concentrations. This is surprising and shows again that it is difficult to predict ion concentrations in the nanopores of protein crystals.

Influence of Space Group, Solvent Content, and Crystal Packing on pH and Ca^{2+} Concentration in the Crystal Nanopores. In general, further experiments will be necessary to study the influence of space group, solvent content, and crystal packing on pH and Ca^{2+} concentration in the crystal nanopores. For example, with the here proposed method, it will be possible to study the influence of different space groups of the same protein. Tetragonal lysozyme crystals can be compared with hexagonal lysozyme crystals,[23] or the different crystal forms of thaumatin[24] can be compared.

Single-Wavelength Indicators Versus Ratiometric Indicators. Here, we use the ratiometric pH-sensitive dye SNARF-1 and the single-wavelength calcium indicator dyes. Ratiometric dyes have the advantage of allowing functional imaging independent of the number of dye molecules. Therefore, the pH in the crystal could be determined with a single measurement after a calibration curve was measured in the bath solution with adjusted pH.

This was not possible with the single-wavelength indicators. For them, a full titration curve has to be measured in the crystal and then fitted with a scaling factor to the calcium calibration curve measured in the bath. This required the assumption that the difference is scaled with a constant factor. The constant pH shift measured independently at different pHs supports this assumption. Also, the good one-parameter fit of the scaling factor in thaumatin and lysozyme nanopores back a constant scaling factor.

Summarizing, ratiometric dyes are preferable, but the scaling factor can also be determined with a single-wavelength indicator. This conclusion increases the number of available probes for functional imaging in protein crystal nanopores dramatically.

CONCLUSIONS

Every protein crystal has its unique pore system and in the future, this pore system could be even designed as soon as protein confirmation and crystallization can be predicted by modeling. This will allow designing specific nanoporous materials from proteins. Functional optical imaging will allow to access and characterize the conditions in the nanopores.

We propose that the described method is not limited to measure calcium and pH in nanopores of protein crystals but can be applied with all other available molecular probes, for example, for Cl^-, Na^+, K^+, Mg^{2+}, Zn^{2+}, Cu^{2+}, Fe^{2+}, Pb^{2+}, Cd^{2+}, and other metal ions with ratiometric and single-wavelength probes. As long as the nanopores are large enough to allow the molecular probe to enter, the method is not limited to protein crystals but can be applied to all transparent nanoporous materials.

AUTHOR INFORMATION

Corresponding Authors

*E-mail: Kazuo.Mori@oist.jp (K.M.).
*E-mail: bkuhn@oist.jp (B.K.).

ORCID

Bernd Kuhn: 0000-0002-6852-2433

Notes

The authors declare no competing financial interest.

ACKNOWLEDGMENTS

We are grateful for the generous support and funding from the Okinawa Institute of Science and Technology Graduate University. We thank Stefan Pommer for the preliminary work.

REFERENCES

(1) Matthews, B. W. Solvent content of protein crystals. *J. Mol. Biol.* **1968**, *33*, 491−497.
(2) Forsythe, E.; Achari, A.; Pusey, M. L. Trace fluorescent labeling for high-throughput crystallography. *Acta Crystallogr., Sect. D: Biol. Crystallogr.* **2006**, *62*, 339−346.
(3) Watts, D.; Müller-Dieckmann, J.; Tsakanova, G.; Lamzin, V. S.; Groves, M. R. Quantitive evaluation of macromolecular crystallization experiments using 1,8-ANS fluorescence. *Acta Crystallogr., Sect. D: Biol. Crystallogr.* **2010**, *66*, 901−908.
(4) Pusey, M.; Barcena, J.; Morris, M.; Singhal, A.; Yuan, Q.; Ng, J. Trace fluorescent labeling for protein crystallization. *Acta Crystallogr., Sect. F: Struct. Biol. Cryst. Commun.* **2015**, *71*, 806−814.
(5) Groves, M. R.; Müller, I. B.; Kreplin, X.; Müller-Dieckmann, J. A method for the general identification of protein crystals in crystallization experiments using a noncovalent fluorescent dye. *Acta Crystallogr., Sect. D: Biol. Crystallogr.* **2007**, *63*, 526−535.
(6) Cvetkovic, A.; Straathof, A. J. J.; Hanlon, D. N.; van der Zwaag, S.; Krishna, R.; van der Wielen, L. A. M. Quantifying anisotropic solute transport in protein crystals using 3-D laser scanning confocal microscopy visualization. *Biotechnol. Bioeng.* **2004**, *86*, 389−398.
(7) Cvetkovic, A.; Zomerdijk, M.; Straathof, A. J. J.; Krishna, R.; van der Wielen, L. A. M. Adsorption of fluorescein by protein crystals. *Biotechnol. Bioeng.* **2004**, *87*, 658−668.
(8) Cvetkovic, A.; Straathof, A. J. J.; Krishna, R.; van der Wielen, L. A. M. Adsorption of xanthene dyes by lysozyme crystals. *Langmuir* **2005**, *21*, 1475−1480.
(9) Khan, I.; Gillilan, R.; Kriksunov, I.; Williams, R.; Zipfel, W. R.; Englich, U. Confocal microscopy on the beamline: novel three-dimensional imaging and sample positioning. *J. Appl. Crystallogr.* **2012**, *45*, 936−943.
(10) Seemann, K. M.; Kiefersauer, R.; Jacob, U.; Kuhn, B. Optical pH detection within a protein crystal. *J. Phys. Chem. B* **2012**, *116*, 9873−9881.
(11) Cvetkovic, A.; Picioreanu, C.; Straathof, A. J. J.; Krishna, R.; van der Wielen, L. A. M. Quantification of binary diffusion in protein crystals. *J. Phys. Chem. B* **2005**, *109*, 10561−10566.
(12) Geremia, S.; Campagnolo, M.; Demitri, N.; Johnson, L. N. Simulation of diffusion time of small molecules in protein crystals. *Structure* **2006**, *14*, 393−400.
(13) Lukk, T.; Gillilan, R. E.; Szebenyi, D. M. E.; Zipfel, W. R. A visible-light-excited fluorescence method for imaging protein crystals without added dyes. *J. Appl. Crystallogr.* **2016**, *49*, 234−240.
(14) Madden, J. T.; DeWalt, E. L.; Simpson, G. J. Two-photon excited UV fluorescence for protein crystal detection. *Acta Crystallogr., Sect. D: Biol. Crystallogr.* **2011**, *67*, 839−846.
(15) Valeur, B.; Berberan-Santos, M. N. *Molecular Fluorescence: Principles and Applications*, 2nd ed.; Wiley-VCH: Weinheim, Germany, 2013; p xix, 569 pages.
(16) Wel, H.; Loeve, K. Isolation and characterization of thaumatin I and II, the sweet-tasting proteins from Thaumatococcus daniellii Benth. *Eur. J. Biochem.* **1972**, *31*, 221−225.

DOI: 10.1021/acs.jpcb.8b07099
J. Phys. Chem. B 2018, 122, 9646−9653

(17) Ogata, C. M.; Gordon, P. F.; de Vos, A. M.; Kim, S.-H. Crystal structure of a sweet tasting protein thaumatin I, at 1·65 Å resolution. *J. Mol. Biol.* **1992**, *228*, 893−908.
(18) Fleming, A. On a remarkable bacteriolytic element found in tissues and secretions. *Proc. R. Soc. B* **1922**, *93*, 306−317.
(19) Blake, C. C. F.; Koenig, D. F.; Mair, G. A.; North, A. C. T.; Phillips, D. C.; Sarma, V. R. Structure of Hen Egg-White Lysozyme: A Three-dimensional Fourier Synthesis at 2 Å Resolution. *Nature* **1965**, *206*, 757−761.
(20) Pollard, T. D. A guide to simple and informative binding assays. *Mol. Biol. Cell* **2010**, *21*, 4061−4067.
(21) Warkentin, M.; Thorne, R. E. Slow cooling of protein crystals. *J. Appl. Crystallogr.* **2009**, *42*, 944−952.
(22) Morozov, V. N.; Kachalova, G. S.; Evtodienko, V. U.; Lanina, N. F.; Morozova, T. Y. Permeability of Lysozyme Tetragonal Crystals to Water. *Eur. Biophys. J.* **1995**, *24*, 93−98.
(23) Brinkmann, C.; Weiss, M. S.; Weckert, E. The structure of the hexagonal crystal form of hen egg-white lysozyme. *Acta Crystallogr., Sect. D: Biol. Crystallogr.* **2006**, *62*, 349−355.
(24) Ko, T. P.; Day, J.; Greenwood, A.; McPherson, A. Structures of three crystal forms of the sweet protein thaumatin. *Acta Crystallogr., Sect. D: Biol. Crystallogr.* **1994**, *50*, 813−825.

DOI: 10.1021/acs.jpcb.8b07099
J. Phys. Chem. B 2018, 122, 9646−9653